

This discussion paper is/has been under review for the journal Atmospheric Chemistry and Physics (ACP). Please refer to the corresponding final paper in ACP if available.

Novel method of generation of $\text{Ca}(\text{HCO}_3)_2$ and CaCO_3 aerosols and first determination of hygroscopic and cloud condensation nuclei activation properties

D. F. Zhao^{1,2}, A. Buchholz², Th. F. Mentel², K.-P. Müller², J. Borchardt²,
A. Kiendler-Scharr², C. Spindler², R. Tillmann², A. Trimborn³, T. Zhu¹, and
A. Wahner²

¹State Key Joint Laboratory of Environmental Simulation and Pollution Control, College of Environmental Sciences and Engineering, Peking University, Beijing, 100871, China

²Forschungszentrum Jülich, Institut für Chemie und Dynamik der Geosphäre–2: Troposphäre, 52425 Jülich, Germany

³Aerodyne Research Inc., 45 Manning Rd, Billerica, MA 01821, USA

Received: 10 March 2010 – Accepted: 11 March 2010 – Published: 26 March 2010

Correspondence to: Th. F. Mentel (t.mentel@fz-juelich.de)

Published by Copernicus Publications on behalf of the European Geosciences Union.

**Hygroscopic and
cloud condensation
nuclei activation
properties**

D. F. Zhao et al.

Title Page

Abstract

Introduction

Conclusions

References

Tables

Figures

⏪

⏩

◀

▶

Back

Close

Full Screen / Esc

Printer-friendly Version

Interactive Discussion

Abstract

Atmospheric mineral aerosols contain CaCO_3 as a reactive component. A novel method to produce CaCO_3 aerosol was developed by spraying $\text{Ca}(\text{HCO}_3)_2$ solutions, which were generated from CaCO_3 suspensions and CO_2 . By aerosol mass spectrometry the freshly sprayed aerosol was characterized to be $\text{Ca}(\text{HCO}_3)_2$ which under annealing in a tube furnace transformed into CaCO_3 . Transmission Electron Microscopy demonstrated that the particles produced were spherical. The method is easy to operate and was able to generate aerosol of sufficient concentration and proper size for the study of physicochemical properties as was demonstrated for hygroscopicity and CCN activity measurements, and investigations of heterogeneous reactions of mineral aerosol. Fresh $\text{Ca}(\text{HCO}_3)_2$ particles are somewhat more hygroscopic than CaCO_3 particles although both have small growth factors of 1.03 and 1.01, respectively, at 95% relative humidity. The CCN activity of $\text{Ca}(\text{HCO}_3)_2$ aerosol is remarkably higher than that of CaCO_3 aerosol and only slightly less than that of $\text{Ca}(\text{NO}_3)_2$. Experiments in the Large Jülich Aerosol Chamber showed that $\text{Ca}(\text{HCO}_3)_2$ can exist for several hours under dry atmospheric conditions which is in contrast to the current believe that $\text{Ca}(\text{HCO}_3)_2$ is unstable in the atmosphere. We conclude that $\text{Ca}(\text{HCO}_3)_2$ maybe be formed in the atmosphere in cloud droplets of activated mineral dust by reaction of CaCO_3 with CO_2 and H_2O . The presence of $\text{Ca}(\text{HCO}_3)_2$ and as a consequence an enhanced CCN activity may alter the influence of mineral aerosol on global climate.

1 Introduction

Mineral aerosol is one of the most abundant components of aerosols in the atmosphere. It mainly arises from wind-blown soil in the deserts or semiarid areas, and also from volcanic dust, road dust and some industrial and agricultural processes. It was estimated that approximately 1000–3000 Tg of mineral aerosols are annually emitted into the atmosphere (Jonas et al., 1995). While mineral aerosol is typically considered

Hygroscopic and cloud condensation nuclei activation properties

D. F. Zhao et al.

Title Page

Abstract

Introduction

Conclusions

References

Tables

Figures

⏪

⏩

◀

▶

Back

Close

Full Screen / Esc

Printer-friendly Version

Interactive Discussion

**Hygroscopic and
cloud condensation
nuclei activation
properties**

D. F. Zhao et al.

Title Page

Abstract

Introduction

Conclusions

References

Tables

Figures

⏪

⏩

◀

▶

Back

Close

Full Screen / Esc

Printer-friendly Version

Interactive Discussion

as having a coarse mode type of distribution, a significant number of mineral particles are also found in the fine mode (Usher, 2003; Song et al., 2005). On the regional scale, mineral dust has an impact on the visibility, air quality, and human health. On the global scale, it can not only influence radiative transfer by absorption and scattering of solar radiation, but also affect the cloud formation and cloud optical properties. Thus, mineral aerosols influence the global climate ultimately by direct and indirect radiative forcing. During long range transport, mineral aerosols can undergo various heterogeneous reactions and their deposition has an impact on the ocean ecosystem and the overall biogeochemical cycling. CaCO_3 is a common component of mineral dust, especially in East Asia and is generally regarded as the most reactive component in mineral particles (Krueger et al., 2003; Laskin et al., 2005; Sullivan et al., 2007; Usher, 2003). It is present at significant concentrations in both the mineral aerosols (Okada et al., 2005; Zhang, 2003) and in the surface soils (at least 5–10% by mass) of most of the major global dust sources (Claquin et al., 1999). It was found that CaCO_3 is among the few “volatile” components in the mineral aerosol which can undergo heterogeneous reactions with atmospheric trace acids to form CO_2 (Krueger et al., 2003; Laskin et al., 2005). Many researchers have investigated the heterogeneous reactions of CaCO_3 as a surrogate for mineral dust and its impact on the physiochemical properties of mineral particles (Krueger et al., 2003; Liu et al., 2008a, b; Gibson et al., 2006a). To study the physiochemical properties of mineral aerosols, the generation of surrogates of mineral aerosol components is often helpful. At present, there are two main methods to generate CaCO_3 aerosols, dry dispersion of solid powders (Sullivan et al., 2009a, b; Prince et al., 2007) and atomizing aqueous suspension of CaCO_3 powder (Gibson et al., 2006, 2007). Both are not easy to handle and it is difficult to generate a stable output of proper size and sufficient mass concentration. Compared to the method of dry dispersion of solid powders, generating aerosol by atomizing solutions does not need complex instrumentation and is easier to operate and control. However, most of the mineral dust components are characterized by very low solubility which makes atomization from solution difficult. Vlasenko et al. (2006) have used atomization of a

**Hygroscopic and
cloud condensation
nuclei activation
properties**

D. F. Zhao et al.

Title Page

Abstract

Introduction

Conclusions

References

Tables

Figures

⏪

⏩

◀

▶

Back

Close

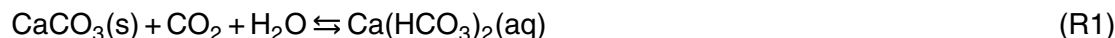
Full Screen / Esc

Printer-friendly Version

Interactive Discussion

saturated solution of CaCO_3 to produce CaCO_3 aerosol. However due to the low solubility of CaCO_3 in water, the number concentration of the obtained aerosol is often not high enough and the size distribution has its maximum at too small diameters considering the need of studies of physiochemical properties, such as hygroscopicity using HTDMA and CCN activation.

In order to study chemical reactions on CaCO_3 particles and to determine microphysical properties of the processed aerosols it would be advantageous to have at disposal an easy to handle and reproducible method for generation of CaCO_3 aerosol with sufficiently high particle concentration at proper size. Here we describe a new, simple method to generate CaCO_3 aerosol by atomization of solutions with enhanced amounts of dissolved CaCO_3 . The basic idea is to make use of the equilibrium of CaCO_3 and the water-soluble form $\text{Ca}(\text{HCO}_3)_2$ in the presence of CO_2 (Reaction R1). This equilibrium is ubiquitous in natural waters when dissolved CO_2 is in contact with rocks containing CaCO_3 . This process of dissolution of CaCO_3 leads e.g. to the formation of stalactites, stalagmites, columns, and other speleothems within caves when CO_2 in the water is lost and CaCO_3 sediment is produced (Fairchild et al., 2006; Murray, 1954).



At high CO_2 concentrations Reaction (R1) will proceed in the forward direction and cause the dissolution of the solid CaCO_3 . On the other hand, when CO_2 is decreasing, the backward reaction will produce solid CaCO_3 . In this study, pure CO_2 was bubbled into a slurry of CaCO_3 powder in order to promote the dissolution of CaCO_3 and formation of a $\text{Ca}(\text{HCO}_3)_2$ solution.

We will show in the following that atomizing $\text{Ca}(\text{HCO}_3)_2$ solutions, drying and annealing of the aerosol promote CaCO_3 formation. The aerosols produced were characterized by Scanning Mobility Particle Sizing, Aerosol Mass Spectrometry, and Transmission Electron Microscopy in order to get the size distribution, typical concentrations, chemical composition and morphology of the aerosol. At the same time, freshly

sprayed and annealed aerosols were characterized with respect to their hygroscopicity and cloud condensation activity (CCN) activity using a Hygroscopicity Tandem Differential Mobility Analyzer (HTDMA) and a Cloud Condensation Nuclei Counter (CCNC) taking advantage of the expected significant difference in solubility between CaCO_3 and $\text{Ca}(\text{HCO}_3)_2$.

To our best knowledge this method of generating CaCO_3 aerosols from a CO_2 containing solution of $\text{Ca}(\text{HCO}_3)_2$ has not been described before. Moreover, not much attention has been paid to the possible importance of $\text{Ca}(\text{HCO}_3)_2$ which could form in the atmosphere in cloud droplets of activated mineral dust containing CaCO_3 by reaction with CO_2 and H_2O .

2 Experimental

2.1 Preparation of $\text{Ca}(\text{HCO}_3)_2$ solution

$\text{Ca}(\text{HCO}_3)_2$ solutions were prepared at room temperature ($\sim 22^\circ\text{C}$) by bubbling CO_2 (Praxair Industriegase GmbH & Co. KG, CO_2 4.5) at a pressure of 20 mbar from the cylinder into 1 L water (Milli-Q, 18.2 Ω) containing 2 g CaCO_3 powder (pro analysis, $\geq 99\%$, Merck). During CO_2 bubbling the slurry was stirred using a magnetic stirrer to promote the suspension of solid CaCO_3 in the water. After bubbling, the slurry was allowed to settle for 5 min and the supernatant clear $\text{Ca}(\text{HCO}_3)_2$ solution was decanted.

In order to characterize the reproducibility of the method and the stability of the solution for aerosol generation, different CO_2 bubbling duration was applied and the solutions were atomized over longer periods. The aerosol was dried and the number density and the count median of the size distribution were determined. It was found that stirring the slurry helped to reach the equilibrium faster.

Hygroscopic and cloud condensation nuclei activation properties

D. F. Zhao et al.

Title Page

Abstract

Introduction

Conclusions

References

Tables

Figures

⏪

⏩

◀

▶

Back

Close

Full Screen / Esc

Printer-friendly Version

Interactive Discussion

2.2 Generation of CaCO₃ particles

The Ca(HCO₃)₂ solution was sprayed by a constant output atomizer (TSI, Model 3076) using synthetic air (Linde LiPur 6.0). The generated aerosol passed through a diffusion drying tube filled with silica gel and a delay tube to equilibrate charges as shown in Fig. 1 (Dinar et al., 2006). The number size distribution of the resulting aerosol was measured by an SMPS system (TSI, DMA 3071, CPC 3022A).

At room temperature Ca(HCO₃)₂ should be unstable as a solid and only exist in solution as Ca²⁺ and HCO₃⁻ (Keiser and Leavitt, 1908; Miller, 1952; House, 1981). Upon drying, it is supposed to convert to CaCO₃ very easily at room temperature. However, as shown in the following, the aerosols generated from spraying Ca(HCO₃)₂ solutions still contained a significant amount of Ca(HCO₃)₂ after drying. We therefore used a tube furnace at 300 °C in order to promote the transformation of Ca(HCO₃)₂ to CaCO₃ aerosol. The temperature of the tube furnace was set to 300 °C because at this temperature Ca(HCO₃)₂ should already decompose to form CaCO₃ (Reaction R2) while CaCO₃ is still stable (Keiser and Leavitt, 1908; Sanders and Gallagher, 2002).



The whole setup as used is shown in Fig. 1. After the delay tube the aerosol was neutralized (TSI, 3077) and size selected by a DMA (TSI, DMA 3071). The size-selected aerosol passed the tube furnace which was either at room temperature or set to 300 °C. After the furnace the aerosol flow was split and directed to the different instruments. A Quadrupole Aerosol Mass Spectrometer (Q-AMS, Aerodyne Research Inc., Jayne et al., 2000) was used to characterize the composition of aerosols. HTDMA and CCNC (Droplet Measurement Technologies, DMT-100) were used to investigate the hygroscopicity and CCN activity.

Title Page

Abstract

Introduction

Conclusions

References

Tables

Figures

⏪

⏩

◀

▶

Back

Close

Full Screen / Esc

Printer-friendly Version

Interactive Discussion

2.3 Characterization of chemical composition and morphology of the aerosol

Chemical characterization of the aerosols was provided by the Q-AMS by measuring H₂O and CO₂ evaporating off the particles. In the Q-AMS a focused particle beam is generated by an aerodynamic lens. This beam impacts the heated surface of a vaporizer which is located in the ionization region of a Quadrupole Mass Spectrometer. The ionization of the vapor is achieved by electron impact ionization with electrons of 70 eV. The Q-AMS is routinely operated in two alternating modes. In the so called MS-mode, the size integrated particle composition is measured. In the so called pToF-mode (particle time of flight mode), the size resolved composition is observed for a set of selected mass to charge ratios (m/z). From the combination of the MS-mode and the pToF-mode data, which were measured alternating with 5 min time resolution, the size dependent chemical composition over the accessible particle size range is retrieved. Details of the mode of operation of the Q-AMS are described in Jayne et al. (2000).

Water, mainly detected on the m/z 18 (H₂O⁺), and CO₂, mainly detected at m/z 44 (CO₂⁺), served to determine the bicarbonate and carbonate content. Water and CO₂ were quantified from the MS spectra as described in Allan et al. (2004). The relative ionization efficiency (RIE) of CO₂ was set to 1.4, for H₂O we applied an RIE of 2 which was recently determined by Mensah et al. (2010). The detection and discrimination of Ca(HCO₃)₂ and CaCO₃ by the Q-AMS was accomplished by tuning the temperature of the vaporizer to 300 °C or 900 °C according to the thermal properties of Ca(HCO₃)₂ and CaCO₃. When the temperature of the vaporizer was set to 300 °C, Ca(HCO₃)₂ in the aerosol decomposed at the vaporizer according to Reaction (R2) and was detected in the form of CO₂ and H₂O. When the temperature of the vaporizer was set to 900 °C, both Ca(HCO₃)₂ and CaCO₃ are decomposed (Reactions R3, R4), whereat Ca(HCO₃)₂ should deliver two CO₂ and one H₂O per formula unit, whereas CaCO₃ is supposed to evaporate only one CO₂ per formula unit.



Hygroscopic and cloud condensation nuclei activation properties

D. F. Zhao et al.

[Title Page](#)[Abstract](#)[Introduction](#)[Conclusions](#)[References](#)[Tables](#)[Figures](#)[⏪](#)[⏩](#)[◀](#)[▶](#)[Back](#)[Close](#)[Full Screen / Esc](#)[Printer-friendly Version](#)[Interactive Discussion](#)



By interplay of the annealing temperature of the tube furnace and the temperature of the vaporizer of the Q-AMS the content of CaCO_3 and $\text{Ca}(\text{HCO}_3)_2$ in the aerosol was determined according to Reactions (R2–R4). (Defacto we bypassed the tube furnace for the measurements at room temperature, i.e. we measured before and after annealing in the tube furnace.)

The particle mass distribution as function of the vacuum aerodynamic diameter was observed in the pToF mode of the Q-AMS. By comparing the modal positions of this particle mass distribution and of the particle volume size distribution calculated from the number size distribution measured by the SMPS, the effective particle density was obtained (DeCarlo et al., 2004).

In order to get information about the morphology of the particles, aerosol was sampled before and after annealing on a copper grid using a home-built aerosol sampling device (Marquardt et al., 1992) and characterized by TEM. In the sampling device, a high voltage was applied and aerosol particles were deposited in the electric field onto the copper grid which was positioned in the centre of the gas flow.

2.4 HTDMA operation

The hygroscopic growth of the particles was measured with a home built HTDMA (Buchholz, 2007). With the first DMA particles were selected from the dried poly-disperse aerosol with an electromobility diameter of 150 nm. The size selected aerosol and the sheath air of the second DMA were humidified at a temperature of 27 °C to almost the same relative humidity (RH) with the sheath air being at slightly higher RH. The second DMA is placed in an insulated box and cooled to 20 °C. Before entering the second DMA both aerosol and sheath air were cooled down to the same temperature and thus the RH increased to its final value. To determine the RH inside the second DMA the absolute humidity was calculated from RH and T data of two Vaisala HMP235 sensors before and after the insulated area. In addition the temperatures

[Title Page](#)[Abstract](#)[Introduction](#)[Conclusions](#)[References](#)[Tables](#)[Figures](#)[⏪](#)[⏩](#)[◀](#)[▶](#)[Back](#)[Close](#)[Full Screen / Esc](#)[Printer-friendly Version](#)[Interactive Discussion](#)

of the air flows inside the insulated area were measured with PT100 sensors directly before or after they entered or left the DMA. For calibration ammonium sulfate aerosol was used.

2.5 CCN operation and evaluation

To determine the CCN activity, the polydisperse aerosol was size selected by scanning a DMA between 10 and 450 nm. For each size bin the total number of particles (CN) was detected with an ultrafine water CPC (UWCPC, TSI3786) and the number of activated particles (CCN) at different supersaturations (SS) was measured in parallel with a continuous flow CCNC (Droplet Measurement Technologies, DMT-100). The ratio of CCN to CN is called activated fraction. Since a DMA selects electromobility diameters, multiply charged particles with accordingly larger diameters entered the CCN counter, too. The fraction of these particles pretends activation at small diameters. For a correct interpretation of activation diameters the fraction of multiple charged particles was calculated according to a natural charge distribution. The activated fraction was then determined for each charge class separately and an error function was fitted to the data. The dry activation diameter (or critical dry diameter, D_{crit}) is the turning point of this distribution.

For each SS at least three scans were performed and the resulting D_{crit} were averaged. For calibration D_{crit} of ammonium sulfate was measured for five different SS.

2.6 Aerosol Chamber experiments

The long term behavior of $\text{Ca}(\text{HCO}_3)_2$ aerosol was studied in the Jülich Large Aerosol Chamber (Mentel et al., 1996). Before any experiment with $\text{Ca}(\text{HCO}_3)_2/\text{CaCO}_3$ we determined the background concentration of HNO_3 in the chamber by sampling a continuous air stream of 1 l/min through a stripping solution (1% CaCl_2 w/w) in a washing bottle. The stripping solution was backed-up by a second washing bottle with the same solution. The nitrate content of the stripping and the backup solution were analyzed

Hygroscopic and cloud condensation nuclei activation properties

D. F. Zhao et al.

Title Page

Abstract

Introduction

Conclusions

References

Tables

Figures

⏪

⏩

◀

▶

Back

Close

Full Screen / Esc

Printer-friendly Version

Interactive Discussion

by ion chromatography. The background HNO_3 concentration was estimated to be 1.1 ± 0.5 ppb at a RH of 30%.

In order to generate the aerosols the solution containing $\text{Ca}(\text{HCO}_3)_2$ was prepared as described above and sprayed by ten two-fluid nozzles against the walls of a small pre-chamber to impact larger droplets (Wahner et al., 1998). The generation air stream of 140 l/min served to flush the submicron portion of the aerosol into the large chamber. This air stream is saturated with water vapor and the aerosol is conditioned in the large chamber by mixing with the chamber air. Nevertheless, the rise RH in the large chamber by the generation air stream is small; typically a flushing for 20 min raised the RH by less than 2% at 290 K.

We performed three types of experiments. In the first experiment the large aerosol chamber was flushed for several hours with dry synthetic air (Linde LiPur 6.0) without CO_2 (final $\text{RH} < 3\%$) and only the aerosol was added in one step. The experiment lasted 36 h and was repeated once wherein the aerosol was monitored for 24 h. In the second experiment the chamber was flushed with particle free outside air leading to a RH of 40%. The aerosol was added to the outside air in two steps with 3 h in between. In the third experiment the chamber was flushed with dry synthetic air without CO_2 , but then humidified by evaporating water (MilliQ) to approximately 40% RH. Initially 370 ppb NO , 100 ppb NO_2 , and 370 ppb O_3 were filled into the chamber and after 2 h the aerosol was added. In all cases we measured the size distribution, CCN activation, hygroscopic growth, and the ratio $\text{Ca}(\text{HCO}_3)_2/\text{CaCO}_3$ by the Q-AMS.

3 Results and discussions

3.1 Size distribution and stability of aerosol generation

Different CO_2 bubbling durations were applied at room temperature to determine the time required for formation of sufficient $\text{Ca}(\text{HCO}_3)_2$ and for the dissolving process to reach equilibrium. For this, the number concentration N_{tot} of the dried aerosol

Hygroscopic and cloud condensation nuclei activation properties

D. F. Zhao et al.

Title Page

Abstract

Introduction

Conclusions

References

Tables

Figures

⏪

⏩

◀

▶

Back

Close

Full Screen / Esc

Printer-friendly Version

Interactive Discussion

generated from the respective solutions served as a measure. N_{tot} increased fast with increasing bubbling duration but leveled off after >2 h of bubbling. After 1 h of CO_2 treatment the aerosol number concentration has reached 80% of the maximum concentration.

To ensure equilibrium CO_2 was bubbled through the stirred, aqueous CaCO_3 suspension for 3 h to prepare the $\text{Ca}(\text{HCO}_3)_2$ solutions. A typical size distribution of aerosol generated from $\text{Ca}(\text{HCO}_3)_2$ solution is shown in Fig. 2. The number concentration peaked at ~ 120 nm with a geometric standard deviation of ~ 1.8 .

The stability of the solution was tested by continuous spraying of the same solution over a longer period. The total number concentration and the count median diameter of the number size distribution served as a measure of stability (Fig. 3). First the number concentration of the aerosol decreased with spraying time and then leveled off after 100 min. Meanwhile, the median size of aerosol decreased gradually from 120 nm to ~ 80 nm over 2 h. During spraying of the solution a white deposit was formed in the storage bottle and the connecting tubes. This can be explained, since the solution was sprayed with synthetic air, free of CO_2 . The solution lost excess CO_2 and solid CaCO_3 was formed. As CaCO_3 deposits from the solution, the concentration of $\text{Ca}(\text{HCO}_3)_2$ aerosol was decreased resulting in a decrease of both the number concentration and median size of the particles.

3.2 Particle density and morphology

The particles were size selected at an electromobility diameter of 150 nm (Fig. 4). The peaks at 150 nm, 233 nm, and 300 nm corresponded to the single, double and triple charged particles. After passing the tube furnace at 300°C , the size of the particles decreased to 138 nm, 216 nm, and 279 nm, respectively.

A corresponding decrease of the vacuum aerodynamic size was observed in the pToF mode of the Q-AMS as can be recognized in Fig. 5. From the mode positions of the mass size distribution ($D_{\text{max va}}$) measured by Q-AMS and of the volume size distribution ($D_{\text{max em}}$) derived from the SMPS data, an effective density (ρ_{eff}) was obtained

Hygroscopic and cloud condensation nuclei activation properties

D. F. Zhao et al.

Title Page

Abstract

Introduction

Conclusions

References

Tables

Figures

◀

▶

◀

▶

Back

Close

Full Screen / Esc

Printer-friendly Version

Interactive Discussion



according to

$$\rho_{\text{eff}} = \frac{D_{\text{max va}}}{D_{\text{max em}}}. \quad (1)$$

The respective ρ_{eff} were $1.83 \pm 0.1 \text{ g/cm}^3$ before the furnace and $1.79 \pm 0.1 \text{ g/cm}^3$ after the furnace, thus the same within the errors. The effective density of the generated aerosol is lower than the bulk density of calcite or aragonite of 2.71 and 2.83 g/cm^3 , respectively, which implies that it is not compact crystalline CaCO_3 .

Transmission Electron Microscopy TEM was used to obtain images of the particles as shown in Fig. 6. Aerosol particles generated from the $\text{Ca}(\text{HCO}_3)_2$ solution were spherical with a heterogeneous distribution of round structures, some of which look like hollow pits on the surface or spherical structures inside. After annealing in the furnace, these round structures became much finer and evenly distributed on the surface implying that the particles restructured during the annealing process.

3.3 Particle chemical composition

The composition of the aerosols was retrieved from the Q-AMS data. Remember, that we alternated the combination of two heated devices: the tube *furnace* at 300° to anneal the aerosols before the Q-AMS measurement and the *vaporizer* of the Q-AMS to flash-evaporate the particles for detection. (We will strictly use these notations *furnace* and *vaporizer* in the following.) We compared the following four combinations (see also Table 1): Q-AMS vaporizer at 300°C probing *before* (case 1) and *after* (case 2) tube furnace at 300°C , Q-AMS vaporizer at 900°C probing *before* (case 3) and *after* (case 4) the tube furnace (operated at 300°C).

The Q-AMS data were converted from mass to mole numbers and normalized to the Ca content retrieved from the respective SMPS data as follows. To get the aerosol mass concentrations, the volume size distributions were integrated from 60 nm – 700 nm and multiplied with ρ_{eff} . Dividing by the molecular weights of $\text{Ca}(\text{HCO}_3)_2$ and CaCO_3 gives the number of moles of the salts thus of Ca per unit volume of air before and

Hygroscopic and cloud condensation nuclei activation properties

D. F. Zhao et al.

Title Page

Abstract

Introduction

Conclusions

References

Tables

Figures

⏪

⏩

◀

▶

Back

Close

Full Screen / Esc

Printer-friendly Version

Interactive Discussion



**Hygroscopic and
cloud condensation
nuclei activation
properties**D. F. Zhao et al.

[Title Page](#)[Abstract](#)[Introduction](#)[Conclusions](#)[References](#)[Tables](#)[Figures](#)[⏪](#)[⏩](#)[◀](#)[▶](#)[Back](#)[Close](#)[Full Screen / Esc](#)[Printer-friendly Version](#)[Interactive Discussion](#)

after the furnace respectively. This is an anticipation of the following results, thus a working hypothesis at this stage. The normalization to Ca as a conserved quantity is very helpful but not crucial for the following analysis. (The normalization to SMPS data compensated for day to day variations in the aerosol concentrations. As will be shown below an analysis based on normalization to the particle mass instead of Ca led to the same results.) Of course it would have been easier to normalize to a Q-AMS internal quantity. However, neither Ca nor total mass of the carbonates can be measured quantitatively by the Q-AMS since the CaO resulting from Reactions (R3) and (R4) is not flash-evaporating completely at Q-AMS vaporizer temperatures of 300 °C or 900 °C. However we can also benefit from the normalization to SMPS based Ca since it allows for testing the collection efficiency (CE) of the Q-AMS. Note already here, that the CE was ~50% in case 1 and 3. The CE was close to 100% in case 4 and cannot be determined for case 2. This will be discussed in more detail below.

The molar ratios CO₂/Ca, H₂O/Ca based on Q-AMS/SMPS and the molar ratio of H₂O to CO₂ based on the Q-AMS data only are shown in Fig. 7 respectively. The error bar represents the standard deviation of repeated measurements. As mentioned above, at the Q-AMS vaporizer temperature of 300 °C we expect to detect Ca(HCO₃)₂ by one CO₂ and one H₂O by the Q-AMS, because of the incomplete thermal decomposition (Reaction R1). At the vaporizer temperature of 900 °C thermal decomposition (Reaction R3) is complete and two CO₂ and one H₂O should be detected. CaCO₃ is not detected at 300 °C but at 900 °C where one CO₂ is formed.

For the aerosol *before* annealing significant amounts of CO₂ were detected at 300 °C Q-AMS vaporizer temperature (case 1, Fig. 7a). The measured amount doubled when the vaporizer was turned to 900 °C (case 3, Fig. 7a). The detected amount of H₂O was the same for both vaporizer temperatures (Fig. 7b). The molar ratio of H₂O to CO₂ was close to 1 at 300 °C and close to 0.5 for 900 °C, respectively (Fig. 7c). This means that before annealing the aerosol consisted of nearly pure Ca(HCO₃)₂ with no additional water in the particles and that all Ca(HCO₃)₂ was destroyed on the vaporizer of the Q-AMS at 300 °C. Nevertheless, the ratios CO₂/Ca and H₂O/Ca in cases 1 and 3 are only

half as large as expected from stoichiometry indicating a reduced CE of the Q-AMS.

For particles that were annealed in the tube furnace to 300 °C neither CO₂ nor H₂O was detected at 300 °C vaporizer temperature (case 2), because all thermally available CO₂ and H₂O were already driven out in the tube furnace (Fig. 7a and b). This also means that after annealing in the furnace, the aerosol consisted of nearly pure CaCO₃. In case 2 small numbers near the detection level were leading to the large errors bars in Fig. 7c. At 900 °C vaporizer temperature (case 4) we observed only a very small amount of H₂O, but a large signal of CO₂ (Fig. 7b and a).

If the particles consisted of pure Ca(HCO₃)₂ before annealing and of pure CaCO₃ thereafter, one CO₂ is lost by conversion of Ca(HCO₃)₂ to CaCO₃ (Reaction R2) in the tube furnace. Therefore we should observe for Q-AMS vaporizer temperatures of 900 °C only half of the CO₂ after annealing. However, comparing the cases 3 and 4 the CO₂ signals before and after annealing have the same magnitude. This cannot be due to incomplete conversion of Ca(HCO₃)₂ to CaCO₃ because only little water is observed in case 4. Also large shape factor effects can be excluded since the particles kept their overall spherical shape after passing the furnace (Fig. 6). The *observed as expected* mole ratios of H₂O/CO₂ in cases 1 and 3 (Fig. 7c) and *the observed as expected* doubling of the CO₂ amount going from case 1 to case 3 excludes simple effects of the different vaporizer temperatures.

The observed CO₂/Ca ratios (Fig. 7a) and H₂O/Ca ratios (Fig. 7b) indicate that the CE of the Q-AMS must have differed between the cases. The data are consistent with a CE of about 50% in cases 1 and 3 and near 100% in case 4. This is dissatisfying. Collection efficiencies for solid particles below 100% have been observed before. This is explained by solid particles bouncing off the vaporizer surface before full evaporation (Matthew et al., 2008). Note in Fig. 5 that our mass distributions were within the transmission window 60–600 nm, and the little tailing at large diameters into the fall off range of the aerodynamic lens cannot cause effects of a factor of two. Unfortunately, we intrinsically cannot observe a signal in case 2. This prevents testing if annealing of the particles at 300 °C and conversion from Ca(HCO₃)₂ to CaCO₃ has led to higher CE.

Hygroscopic and cloud condensation nuclei activation properties

D. F. Zhao et al.

Title Page

Abstract

Introduction

Conclusions

References

Tables

Figures



Back

Close

Full Screen / Esc

Printer-friendly Version

Interactive Discussion

However, higher CE for tempered solid particles compared to freshly dried particles seems to be anyhow somewhat anti-intuitive. We repeated the experiments with virtually the same results, i.e. enhanced CO_2 and CE in case 4 is not a singular artifact. It remains unexplained for the moment, but adds only little uncertainty to our findings. All other evidence supports that we produced $\text{Ca}(\text{HCO}_3)_2$ aerosol by spraying the solution and that we were able to convert it to CaCO_3 by annealing it to 300°C .

The general composition of the generated carbonate aerosols can be written as $x\text{Ca}(\text{HCO}_3)_2 \cdot y\text{CaCO}_3 \cdot z\text{H}_2\text{O}$. The combination of furnace temperature and the Q-AMS vaporizer temperature and the corresponding species detected are listed in Table 1. If the total calcium salt is normalized to unity, then y equals $1-x$. Then x , y , z can be obtained from the Eqs. (2–7):

$$\frac{n_{n\text{CO}_2}(900^\circ)}{n_{n\text{CO}_2}(300^\circ)} = \frac{1+x}{x} \quad (2)$$

$$r_1 = \frac{n_{n\text{CO}_2}(900^\circ)}{n_{n\text{CO}_2}(300^\circ)} \quad (3)$$

$$x = \frac{1}{r_1 - 1} \quad (4)$$

$$\frac{n_{n\text{H}_2\text{O}}(300^\circ)}{n_{n\text{CO}_2}(300^\circ)} = \frac{x+z}{x} \quad (5)$$

$$r_2 = \frac{n_{n\text{H}_2\text{O}}(300^\circ)}{n_{n\text{CO}_2}(300^\circ)} \quad (6)$$

$$z = (r_2 - 1) \cdot x \quad (7)$$

Herein $n_{n\text{CO}_2}(900^\circ)$ is the mole number of CO_2 in the aerosol *normalized* to the aerosol mass concentration before annealing (22°C) detected at 900°C in the AMS and $n_{n\text{H}_2\text{O}}$

Hygroscopic and cloud condensation nuclei activation properties

D. F. Zhao et al.

Title Page

Abstract

Introduction

Conclusions

References

Tables

Figures

⏪

⏩

◀

▶

Back

Close

Full Screen / Esc

Printer-friendly Version

Interactive Discussion



(300°) and $n_{n\text{CO}_2}$ (300°) are the mole numbers of H₂O and CO₂ normalized in the same way but detected at 300 °C in the AMS.

The composition of the aerosol before and after annealing was determined this way and is shown in Table 2. For the aerosol before the furnace, x was near unity and y and z were zero within the error limits (the value of x should be less than or equal to 1 and x , y , z should be positive) which means almost the whole particle consisted of Ca(HCO₃)₂. The ratio of z to x was near zero indicating there is no additional water. In contrast, after the furnace, the particle consists of almost pure CaCO₃ with very little Ca(HCO₃)₂ left. This is consistent with the analysis discussed above.

From the composition of the aerosol in Table 2, the mass concentration of CO₂, H₂O normalized to the aerosol mass concentration were calculated as a theoretical value and compared the with measured value (Table 3). The ratio of measured to calculated concentrations gives an estimate of CE supporting the above mentioned values of ~50% in cases 1 and 3 and of 100% in case 4.

Based on the analysis of the composition of the aerosol above, we will refer to the aerosol before annealing in the furnace as Ca(HCO₃)₂ aerosol and to the aerosol after annealing as CaCO₃ aerosol in the following discussion.

3.4 Hygroscopicity of the aerosol

The humidograms of the laboratory generated aerosols are shown in Fig. 8. CaCO₃ aerosol (red) took up only very little water at very high RH and deliquescence was not observed up to RH of 97.4(±1.4) %. Ca(HCO₃)₂ (dark blue) showed a different growth behavior. Up to RH of 68.2(±1.4) % the particle diameter increased by 1%. Between 68% and 77% the growth factor (GF) decreased and reached a minimum of 0.95 at RH 89.5(±1.4)%. Thereafter the particles grew continuously with increasing RH without showing a distinct deliquescence point. Condensation of small amounts of water (GF=1.01 at 68% RH) obviously caused shrinking of the particles probably due to some water aided restructuring of the particles (compare the TEM image in Fig. 6a). Shape effects can be excluded since the dried particles were already spherical. To

Hygroscopic and cloud condensation nuclei activation properties

D. F. Zhao et al.

Title Page

Abstract

Introduction

Conclusions

References

Tables

Figures

⏪

⏩

◀

▶

Back

Close

Full Screen / Esc

Printer-friendly Version

Interactive Discussion



**Hygroscopic and
cloud condensation
nuclei activation
properties**

D. F. Zhao et al.

[Title Page](#)[Abstract](#)[Introduction](#)[Conclusions](#)[References](#)[Tables](#)[Figures](#)[⏪](#)[⏩](#)[◀](#)[▶](#)[Back](#)[Close](#)[Full Screen / Esc](#)[Printer-friendly Version](#)[Interactive Discussion](#)

test the effect of wetting the particles, the dry aerosol was humidified to almost 100% and then dried again before entering the instruments. After the wet-conditioning the minimum in the growth curve disappeared and the particles did not grow until ca. 92% (Fig. 8, light blue). The uptake of water already occurred at lower RH and was higher than for CaCO_3 . No distinct deliquescence point was observed. When the growth curve of the non-conditioned aerosol was shifted using the diameter of the minimum at RH 89.5% as reference diameter (Fig. 8, middle blue), the high humidity branches at $\text{RH} > 93\%$ for the particles with and without wet-conditioning agree within the errors, thus should have the same composition and morphology.

The Q-AMS analysis showed that the wet-conditioned particles consisted of $\sim 67\%$ CaCO_3 and $\sim 33\%$ $\text{Ca}(\text{HCO}_3)_2$. The conditioning process can be imagined as dissolving some bicarbonate in the water layer, where it decays and CO_2 evaporates. This is the same process as occurring in weathering of carbonate rocks. In comparison to the pure CaCO_3 , the presence of $\text{Ca}(\text{HCO}_3)_2$ increased the growth factors and thus shifted the growth curve to lower RH. $\text{Ca}(\text{HCO}_3)_2$ seemed to be unstable at $\text{RH} > 68\%$ even on the short time scales of the HTDMA measurement. Because of this instability the growth behavior of pure $\text{Ca}(\text{HCO}_3)_2$ could not be determined. However, it should be much more hygroscopic than the mixed salt as indicated by the GF at RH 70%.

3.5 CCN activity of aerosol

We determined the dry diameter of those particles which are activated at a given supersaturation (SS) with a CCN counter. We will call this the critical dry diameter (D_{crit}) which is different from another often used definition of D_{crit} as diameter of the droplet at the maximum of the Köhler curve. The measured D_{crit} are shown in Fig. 9. CaCO_3 particles (red filled circles) activated at significantly larger diameters than the $\text{Ca}(\text{HCO}_3)_2$ particles (light and dark blue circles) before annealing. The D_{crit} of our spray-annealed CaCO_3 agreed very well with observations of Sullivan et al. (2009b) who measured CaCO_3 aerosol generated by dispersing dry powder (open red circles).

**Hygroscopic and
cloud condensation
nuclei activation
properties**

D. F. Zhao et al.

[Title Page](#)[Abstract](#)[Introduction](#)[Conclusions](#)[References](#)[Tables](#)[Figures](#)[⏪](#)[⏩](#)[◀](#)[▶](#)[Back](#)[Close](#)[Full Screen / Esc](#)[Printer-friendly Version](#)[Interactive Discussion](#)

To our best knowledge there are no studies of the activation of $\text{Ca}(\text{HCO}_3)_2$ as it was always thought to be too unstable under atmospheric conditions. We found that $\text{Ca}(\text{HCO}_3)_2$ particles are much better CCN than CaCO_3 particles and only a little less active than $\text{Ca}(\text{NO}_3)_2$ (green symbols in Fig. 9, taken from Sullivan et al., 2009b).

5 The pre-conditioning of the $\text{Ca}(\text{HCO}_3)_2$ with water did not cause large effects on the CCN activity at $\text{SS} > 0.25$ (compare light and dark blue circles in Fig. 9). Only at $\text{SS} < 0.25$ the pre-processed particles activate at lower D_{crit} thus are obviously better CCN than pure $\text{Ca}(\text{HCO}_3)_2$ despite the larger fraction of CaCO_3 . Considering the vertical error bars for the adjusted SS in Fig. 9, the data points for pre-conditioned and
10 non-conditioned $\text{Ca}(\text{HCO}_3)_2$ may also belong to a common curve.

$\text{Ca}(\text{HCO}_3)_2$ is the expected product of the reaction of CaCO_3 with CO_2 and H_2O , which have high concentrations in the atmosphere. Thus, especially in cloud droplets of activated mineral dust some $\text{Ca}(\text{HCO}_3)_2$ may be formed. Several studies on the water soluble inorganic ions in aerosols conducted during ACE-Asia have suggested
15 the co-existence of Ca and carbonate/bicarbonate based on the high correlation between Ca^{2+} and the difference of total cations and anions (Maxwell-Meier et al., 2004; Song et al., 2005). Unfortunately, carbonate and bicarbonate were not measured and could not be differentiated in the particle-into-liquid sampler coupled to a dual-channel ion chromatograph (PILS-IC). The significant enhancement of CCN activity going from
20 CaCO_3 to $\text{Ca}(\text{HCO}_3)_2$ indicates that CaCO_3 could become much more CCN active by natural processes especially in remote area when the heterogeneous reactions with pollutant trace gases are negligible.

3.6 Long term experiments in the Large Jülich Aerosol Chamber

$\text{Ca}(\text{HCO}_3)_2$ was introduced into the Large Aerosol Chamber and kept there for up to
25 36 h. CCN activation, hygroscopic growth factors and chemical composition by Q-AMS were monitored to capture the long time evolution of the carbonate aerosol under dry and humid conditions.

**Hygroscopic and
cloud condensation
nuclei activation
properties**

D. F. Zhao et al.

Title Page

Abstract

Introduction

Conclusions

References

Tables

Figures

⏪

⏩

◀

▶

Back

Close

Full Screen / Esc

Printer-friendly Version

Interactive Discussion

The critical diameters D_{crit} of the carbonate particles are shown in Fig. 10. In the two dry experiments D_{crit} was 127 nm directly after generating the $\text{Ca}(\text{HCO}_3)_2$ aerosol, which is about the expected value for $\text{Ca}(\text{HCO}_3)_2$ according to our laboratory scale study above. During the first few hours the activation diameter increased to 150 nm and stayed constant thereafter for the next 5 h. The results of the two experiments differ in that the red curve approaches the final value of 150 nm within 2 h and stays constant thereafter, whereas the black curve took somewhat longer to reach the same value. After 10 h the black curve started to rise again and reached values of 170 nm within 6 h. We have no explanation for this different behavior, which is not related to changes of RH or T in the chamber. However, we can state that even after 22 h/36 h the D_{crit} of 150 nm/170 nm at 0.2% SS were somewhat higher than the 130 nm at 0.2% SS for wet pre-conditioned $\text{Ca}(\text{HCO}_3)_2$. Also, the chamber particles are much better CCN than pure CaCO_3 particles where a SS of $\sim 0.85\%$ was needed to activate particles with D_{crit} of 150 nm.

Since the tendency for droplet activation was lower than that of pre-processed $\text{Ca}(\text{HCO}_3)_2$ one would expect that the hygroscopic growth is also smaller. However, as is shown in Fig. 11 the aerosol from the chamber (different shades of blue circles) had significantly higher GF than the pre-conditioned $\text{Ca}(\text{HCO}_3)_2$ (green circles). Still, at 95% RH the GF is only 1.165. The Q-AMS data showed that the aerosol in the dry chamber contained $\sim 40\%$ $\text{Ca}(\text{HCO}_3)_2$, whereas the pre-processed $\text{Ca}(\text{HCO}_3)_2$ aerosol contained only 33% bicarbonate. We detected some nitrate uptake of background HNO_3 , which was initially about 2% of the CO_2^+ mass and increased slowly to about 4% of the CO_2^+ within 12 h.

These observations can be rationalized by the following considerations. Upon spraying the $\text{Ca}(\text{HCO}_3)_2$ solution and drying it by mixing with the dry air in the chamber primarily $\text{Ca}(\text{HCO}_3)_2$ aerosol was formed. Favored by the low RH and CO_2 free synthetic air in the chamber the particles lost water and CO_2 over several hours and were slowly converted to the thermodynamically stable CaCO_3 . However, even after 36 h the particles were much better CCN (D_{crit} 150 nm or 170 nm at 0.2% SS, respectively)

**Hygroscopic and
cloud condensation
nuclei activation
properties**

D. F. Zhao et al.

Title Page

Abstract

Introduction

Conclusions

References

Tables

Figures

⏪

⏩

◀

▶

Back

Close

Full Screen / Esc

Printer-friendly Version

Interactive Discussion

than CaCO_3 ($D_{\text{crit}}=150$ nm at $\sim 0.85\%$ SS). Therefore a large portion of $\text{Ca}(\text{HCO}_3)_2$ was still left in the particles. This is supported by Q-AMS data that showed that after 14 h the $\text{Ca}(\text{HCO}_3)_2$ accounted still for $\sim 40\%$ of the total calcium salt. Very little gas-phase HNO_3 (2%) was taken up instantaneously by the fresh aerosols. Thereafter nitrate increased only slowly in the dry experiments and had obviously no or small influence; since the D_{crit} increased with time. We suggest that the surface of the particles reacted quickly according to Reaction (R1), protecting the core of the particles from further conversion. Thus after the relatively fast initial rise the activation diameter increased only slowly. Overall $\text{Ca}(\text{HCO}_3)_2$ existed much longer under dry conditions and at room temperature than commonly expected from its thermodynamic stability. Based on the significant difference in CCN activity between $\text{Ca}(\text{HCO}_3)_2$ and CaCO_3 , a longer existence of $\text{Ca}(\text{HCO}_3)_2$ could have important implications for the influence of mineral aerosol on climate.

In the humid chamber (flushed with particle free outside air) D_{crit} reached 135 nm within the first 15 min (blue curve in Fig. 10) which is about the expected value for $\text{Ca}(\text{HCO}_3)_2$. Thereafter we observed a fast decrease. A second addition of fresh aerosols induced the same behavior. After 20 h activation diameters of $92(\pm 3)$ nm were reached which were only slightly higher than the $87.5(\pm 3)$ nm for pure $\text{Ca}(\text{NO}_3)_2$ according to Sullivan et al. (2009b) (black dashed line in Fig. 10).

In the second humid experiment NO , NO_2 and O_3 were added on purpose to the aerosols. The alkaline $\text{Ca}(\text{HCO}_3)_2$ then obviously reacted with NO_2 and HNO_3 to $\text{Ca}(\text{NO}_3)_2$. D_{crit} showed the same fast decay and approached the $\text{Ca}(\text{NO}_3)_2$ values as described above (green curve in Fig. 10).

Also the GF at 90% RH increased rapidly with time and then levelled off (Table 4). The water uptake represented as growth curves (Fig. 11, red and orange) was significantly lower than the water uptake measured for pure $\text{Ca}(\text{NO}_3)_2$ by Gibson et al. (2006), who find a GF already of 1.77 at 85% RH.

In both humid experiments increasing nitrate was detected by the Q-AMS, which replaced HCO_3^- . This is demonstrated in Fig. 12 for the experiment with NO , NO_2 ,

**Hygroscopic and
cloud condensation
nuclei activation
properties**

D. F. Zhao et al.

Title Page

Abstract

Introduction

Conclusions

References

Tables

Figures

⏪

⏩

◀

▶

Back

Close

Full Screen / Esc

Printer-friendly Version

Interactive Discussion

and O_3 addition. However, even after 23 h, still a little $Ca(HCO_3)_2$ and a significant $CaCO_3$ fraction can be detected by switching the vaporizer temperature of the AMS between $900^\circ C$ and $300^\circ C$. Together the carbonate (including bicarbonate) contributed about $\sim 36\%$ of total calcium salt. Nitrate related calcium was determined to account for $\sim 64\%$ (molar content) of the total calcium salt. The total volume of the aerosol increased during the first seven hours. Nitrate and water uptake and overcompensated the chamber losses (Fig. 12).

These observations demonstrated that a substantial heterogeneous conversion into the more soluble $Ca(NO_3)_2$ occurred. We suggest that in early stages of the experiment this took only place on the surface of the particles. But since the nitrate is much more hygroscopic than both, carbonate and bicarbonate, the particles took up water forming a concentrated solution on the surface (Krueger et al., 2003). This further increased the uptake of HNO_3 which is larger on wet particles (Liu et al., 2008a) and also dissolved the upper layers of carbonate. The conversion of $Ca(HCO_3)_2$ to $Ca(NO_3)_2$ thus was accelerated and the reaction of bicarbonate to carbonate was promoted as no protective layer was formed. Carbonate/bicarbonate decreased as the reaction proceeded but were not completely depleted over the time period of the chamber experiment. Therefore the hygroscopic growth was lower than that of pure nitrate. The droplet activation of chamber particles at the final stages was only slightly less than that of pure $Ca(NO_3)_2$ as the reaction to nitrate was much faster than that conversion to carbonate.

4 Conclusions

In this study, a novel, easy to operate method was developed using atomization to produce $CaCO_3$ aerosol, one of the most reactive components in mineral aerosol. In this procedure CO_2 was bubbled through a slurry of $CaCO_3$ dissolving it as bicarbonate. The supernatant solution was decanted, sprayed with an atomizer and dried. Annealing the aerosol in a tube furnace at $300^\circ C$ promoted the conversion back to $CaCO_3$. The method can be used to generate $CaCO_3$ aerosol of sufficiently high concentration and

**Hygroscopic and
cloud condensation
nuclei activation
properties**

D. F. Zhao et al.

[Title Page](#)[Abstract](#)[Introduction](#)[Conclusions](#)[References](#)[Tables](#)[Figures](#)[⏪](#)[⏩](#)[◀](#)[▶](#)[Back](#)[Close](#)[Full Screen / Esc](#)[Printer-friendly Version](#)[Interactive Discussion](#)

proper size for studies of hygroscopicity, CCN activity and aerosol chemistry studies in simulation chambers. Q-AMS measurements confirmed that the aerosol generated with this method consists of $\text{Ca}(\text{HCO}_3)_2$ after drying and is transformed to CaCO_3 in the tube furnace. TEM showed that both the $\text{Ca}(\text{HCO}_3)_2$ and CaCO_3 particles are spherical, with $\text{Ca}(\text{HCO}_3)_2$ particles having some internal structures, bubbles or hollow pits. $\text{Ca}(\text{HCO}_3)_2$ aerosol is more hygroscopic than CaCO_3 although both of them did not exhibit large growth factors (at RH 90%). The $\text{Ca}(\text{HCO}_3)_2$ particles were much better CCN than CaCO_3 particles and only a little less active than $\text{Ca}(\text{NO}_3)_2$. Chamber experiments showed that $\text{Ca}(\text{HCO}_3)_2$ can exist longer under atmospheric conditions than conventionally expected from its thermodynamic stability, especially under dry conditions. In the atmosphere $\text{Ca}(\text{HCO}_3)_2$ can be formed through the reaction of CaCO_3 with CO_2 and H_2O , in particular in cloud droplets of activated mineral. A significant increase of CCN activity in going from CaCO_3 to $\text{Ca}(\text{HCO}_3)_2$ by natural processes may alter the role of mineral aerosols in cloud formation, therefore eventually modifying the impact of mineral aerosol on global climate, especially in remote areas where competing heterogeneous reactions with pollutant trace gases are missing. $\text{Ca}(\text{HCO}_3)_2$ may be present in the atmosphere for longer times, and likely is faster converted into water soluble salts (e.g. nitrates) than CaCO_3 .

Acknowledgements. The authors thank the support of the Junior Scientist Exchange Program between the China Scholarship Council and the Helmholtz Association of German Research Centers.

References

Allan, J. D., Delia, A. E., Coe, H., Bower, K. N., Alfarra, M. R., Jimenez, J. L., Middlebrook, A. M., Drewnick, F., Onasch, T. B., Canagaratna, M. R., Jayne, J. T., and Worsnop, D. R.: A generalised method for the extraction of chemically resolved mass spectra from aerodyne aerosol mass spectrometer data, *J. Aerosol Sci.*, 35, 909–922, 2004.

**Hygroscopic and
cloud condensation
nuclei activation
properties**D. F. Zhao et al.

[Title Page](#)[Abstract](#)[Introduction](#)[Conclusions](#)[References](#)[Tables](#)[Figures](#)[⏪](#)[⏩](#)[◀](#)[▶](#)[Back](#)[Close](#)[Full Screen / Esc](#)[Printer-friendly Version](#)[Interactive Discussion](#)

Buchholz, A.: Entwicklung eines Geräts zur Untersuchung des hygroroskopischen Wachstums von organischen Aerosolen, Diploma Thesis, Department of Chemistry, University of Cologne, Cologne, 2007.

Claquin, T., Schulz, M., and Balkanski, Y. J.: Modeling the mineralogy of atmospheric dust sources, *J. Geophys. Res.*, 104, 22243–22256, 1999.

DeCarlo, P. F., Slowik, J. G., Worsnop, D. R., Davidovits, P., and Jimenez, J. L.: Particle morphology and density characterization by combined mobility and aerodynamic diameter measurements. Part 1: Theory, *Aerosol Sci. Technol.*, 38, 1185–1205, 2004.

Dinar, E., Mentel, T. F., and Rudich, Y.: The density of humic acids and humic like substances (HULIS) from fresh and aged wood burning and pollution aerosol particles, *Atmos. Chem. Phys.*, 6, 5213–5224, 2006,
<http://www.atmos-chem-phys.net/6/5213/2006/>.

Fairchild, I. J., Smith, C. L., Baker, A., Fuller, L., Spottl, C., Matthey, D., and McDermott, F.: Modification and preservation of environmental signals in speleothems, *Earth-Science Rev.*, 75, 105–153, 2006.

Gibson, E. R., Hudson, P. K., and Grassian, V. H.: Physicochemical properties of nitrate aerosols: Implications for the atmosphere, *J. Phys. Chem. A*, 110, 11785–11799, 2006.

Gibson, E. R., Gierlus, K. M., Hudson, P. K., and Grassian, V. H.: Generation of internally mixed insoluble and soluble aerosol particles to investigate the impact of atmospheric aging and heterogeneous processing on the CCN activity of mineral dust aerosol, *Aerosol Sci. Technol.*, 41, 914–924, 2007.

House, W. A.: Kinetics of crystallization of calcite from calcium bicarbonate solutions, *J. Chem. Soc. Farad. Trans. I*, 77, 341–359, 1981.

Jayne, J. T., Leard, D. C., Zhang, X. F., Davidovits, P., Smith, K. A., Kolb, C. E., and Worsnop, D. R.: Development of an aerosol mass spectrometer for size and composition analysis of submicron particles, *Aerosol Sci. Technol.*, 33, 49–70, 2000.

Jonas, P. R., Charlson, R. J., and Rodle, H.: *Climate change 1994: Radiation of Climate Change and An Evaluation of the Changes*, Cambridge University Press, Cambridge, 1995.

Keiser, E. H., and Leavitt, S.: On the preparation and the composition of the acid carbonates of calcium and barium, *J. Am. Chem. Soc.*, 30, 1711–1714, 1908.

**Hygroscopic and
cloud condensation
nuclei activation
properties**

D. F. Zhao et al.

Title Page

Abstract

Introduction

Conclusions

References

Tables

Figures

⏪

⏩

◀

▶

Back

Close

Full Screen / Esc

Printer-friendly Version

Interactive Discussion

- Krueger, B. J., Grassian, V. H., Laskin, A., and Cowin, J. P.: The transformation of solid atmospheric particles into liquid droplets through heterogeneous chemistry: Laboratory insights into the processing of calcium containing mineral dust aerosol in the troposphere, *Geophys. Res. Lett.*, 30, 4, L1148, doi:10.1029/2002GL016563, 2003.
- 5 Laskin, A., Iedema, M. J., Ichkovich, A., Graber, E. R., Taraniuk, I., and Rudich, Y.: Direct observation of completely processed calcium carbonate dust particles, *Farad. Discuss.*, 130, 453–468, 2005.
- Liu, Y., Gibson, E. R., Cain, J. P., Wang, H., Grassian, V. H., and Laskin, A.: Kinetics of heterogeneous reaction of CaCO_3 particles with gaseous HNO_3 over a wide range of humidity, *J. Phys. Chem. A*, 112, 1561–1571, 2008a.
- 10 Liu, Y. J., Zhu, T., Zhao, D. F., and Zhang, Z. F.: Investigation of the hygroscopic properties of $\text{Ca}(\text{NO}_3)_2$ and internally mixed $\text{Ca}(\text{NO}_3)_2/\text{CaCO}_3$ particles by micro-Raman spectrometry, *Atmos. Chem. Phys.*, 8, 7205–7215, 2008b, <http://www.atmos-chem-phys.net/8/7205/2008/>.
- 15 Marquardt, A., Hackfort, H., Borchardt, J., Schober, T., Friedrich, J.: TEM-Untersuchungen der Mikrostrukturen von Verbrennungsaerosolen, *Berichte des Forschungszentrums Jülich*, JUEL-2700, ISSN 0366-0885, 1992.
- Matthew, B. M., Middlebrook, A. M., and Onasch, T. B.: Collection efficiencies in an Aerodyne Aerosol Mass Spectrometer as a function of particle phase for laboratory generated aerosols, *Aerosol Sci. Technol.*, 42, 884–898, doi:10.1080/02786820802356797, 2008.
- 20 Maxwell-Meier, K., Weber, R., Song, C., Orsini, D., Ma, Y., Carmichael, G. R., and Streets, D. G.: Inorganic composition of fine particles in mixed mineral dust-pollution plumes observed from airborne measurements during ACE-Asia, *J. Geophys. Res.-Atmos.*, 109, 20, D19s07, doi:10.1029/2003jd004464, 2004.
- 25 Mensah, A. A., Buchholz, A., Mentel, Th. F., Tillmann, R. and Kiendler-Scharr, A.: Determination of the relative ionization efficiency of water in an Aerodyne aerosol mass spectrometer, *J. Aerosol Sci.*, submitted, 2010.
- Mentel, T. F., Bleilebens, D., and Wahner, A.: A study of nighttime nitrogen oxide oxidation in a large reaction chamber – The fate of NO_2 , N_2O_5 , HNO_3 , and O_3 at different humidities, *Atmos. Environ.*, 30, 4007–4020, 1996.
- 30 Miller, J. P.: A portion of the system calcium carbonate-carbon dioxide-water, with geological implications, *Am. J. Sci.*, 250, 161–203, 1952.
- Murray, J. W.: The deposition of Calcite and Aragonite in caves, *J. Geol.*, 62, 481–492, 1954.

**Hygroscopic and
cloud condensation
nuclei activation
properties**

D. F. Zhao et al.

Title Page

Abstract

Introduction

Conclusions

References

Tables

Figures

◀

▶

◀

▶

Back

Close

Full Screen / Esc

Printer-friendly Version

Interactive Discussion

- Okada, K., Qin, Y., and Kai, K.: Elemental composition and mixing properties of atmospheric mineral particles collected in Hohhot, China, *Atmos. Res.*, 73, 45–67, 2005.
- Prince, A. P., Grassian, V. H., Kleiber, P., and Young, M. A.: Heterogeneous conversion of calcite aerosol by nitric acid, *Phys. Chem. Chem. Phys.*, 9, 622–634, 2007.
- 5 Sanders, J. P. and Gallagher, P. K.: Kinetic analyses using simultaneous TG/DSC measurements Part I: decomposition of calcium carbonate in argon, *Thermochim. Acta*, 388, 115–128, 2002.
- Song, C. H., Maxwell-Meier, K., Weber, R. J., Kapustin, V., and Clarke, A.: Dust composition and mixing state inferred from airborne composition measurements during ACE-Asia C130 Flight #6, *Atmos. Environ.*, 39, 359–369, 2005.
- 10 Sullivan, R. C., Guazzotti, S. A., Sodeman, D. A., and Prather, K. A.: Direct observations of the atmospheric processing of Asian mineral dust, *Atmos. Chem. Phys.*, 7, 1213–1236, 2007, <http://www.atmos-chem-phys.net/7/1213/2007/>.
- Sullivan, R. C., Moore, M. J. K., Petters, M. D., Kreidenweis, S. M., Roberts, G. C., and Prather, K. A.: Timescale for hygroscopic conversion of calcite mineral particles through heterogeneous reaction with nitric acid, *Phys. Chem. Chem. Phys.*, 11, 7826–7837, 2009a.
- 15 Sullivan, R. C., Moore, M. J. K., Petters, M. D., Kreidenweis, S. M., Roberts, G. C., and Prather, K. A.: Effect of chemical mixing state on the hygroscopicity and cloud nucleation properties of calcium mineral dust particles, *Atmos. Chem. Phys.*, 9, 3303–3316, 2009b, <http://www.atmos-chem-phys.net/9/3303/2009/>.
- 20 Usher, C. R., Michel, A. E., and Grassian, V. H.: Reactions on mineral dust, *Chem. Rev.*, 103, 4883–4939, 2003.
- Vlasenko, A., Sjogren, S., Weingartner, E., Stemmler, K., Gggeler, H. W., and Ammann, M.: Effect of humidity on nitric acid uptake to mineral dust aerosol particles, *Atmos. Chem. Phys.*, 6, 2147–2160, 2006, <http://www.atmos-chem-phys.net/6/2147/2006/>.
- 25 Wahner, A., Mentel, T. F., and Sohn, M.: Gas-phase reaction of N_2O_5 with water vapor: Importance of heterogeneous hydrolysis of N_2O_5 and surface desorption of HNO_3 in a large teflon chamber, *Geophys. Res. Lett.*, 25, 2169–2172, 1998.
- 30 Zhang, X. Y., Gong, S. L., Shen, Z. X., Mei, F. M., Xi, X. X., Liu, L. C., Zhou, Z. J., Wang, D., Wand, Y. Q., and Cheng, Y.: Characterization of soil dust aerosol in China and its transport and distribution during 2001 ACE-Asia: 1. Network observations, *J. Geophys. Res.*, 108(13), 4621, doi:10.1029/2002JD002632, 2003.

Hygroscopic and cloud condensation nuclei activation properties

D. F. Zhao et al.

Table 1. Species detected at different temperatures T of tube furnace and Q-AMS vaporizer.

Case No.	T_{furnace}	$T_{\text{vaporizer}}$	Species detected	n_{CO_2}	$n_{\text{H}_2\text{O}}$
1	22 °C (bypass)	300 °C	Ca(HCO ₃) ₂ before furnace (Reaction R2)	x	$x+z$
2	300 °C	300 °C	Ca(HCO ₃) ₂ after furnace (Reaction R2)	no	no
3	22 °C (bypass)	900 °C	Ca(HCO ₃) ₂ +CaCO ₃ before furnace (Reaction R3, R4)	$2x + y$	$x+z$
4	300 °C	900 °C	Ca(HCO ₃) ₂ + CaCO ₃ after furnace (Reaction R3,R4)	$x+y$	no

n_{CO_2} and $n_{\text{H}_2\text{O}}$: detectable mole numbers of CO₂ and H₂O per formula unit of $x\text{Ca}(\text{HCO}_3)_2 \cdot y\text{CaCO}_3 \cdot z\text{H}_2\text{O}$.

[Title Page](#)
[Abstract](#)
[Introduction](#)
[Conclusions](#)
[References](#)
[Tables](#)
[Figures](#)
[Back](#)
[Close](#)
[Full Screen / Esc](#)
[Printer-friendly Version](#)
[Interactive Discussion](#)

**Hygroscopic and
cloud condensation
nuclei activation
properties**

D. F. Zhao et al.

Table 2. Composition of aerosol before and after the furnace.

	$T_{\text{furnace}} [^{\circ}\text{C}]$	x	y	z
Before furnace	22	1.05	-0.05	-0.032
After furnace	300	0.027	0.97	-

[Title Page](#)[Abstract](#)[Introduction](#)[Conclusions](#)[References](#)[Tables](#)[Figures](#)[I◀](#)[▶I](#)[◀](#)[▶](#)[Back](#)[Close](#)[Full Screen / Esc](#)[Printer-friendly Version](#)[Interactive Discussion](#)

Hygroscopic and cloud condensation nuclei activation properties

D. F. Zhao et al.

Table 3. Measured and calculated normalized mass $m_n(\text{CO}_2)$ and $m_n(\text{H}_2\text{O})$.

Case No	$T_{\text{VAPORIZER}}$	measured $m_n(\text{CO}_2)$	calc. $m_n(\text{CO}_2)$	meas. /calc.	measured $m_n(\text{H}_2\text{O})$	calc. $m_n(\text{H}_2\text{O})$	meas. /calc.
1	300 °C before furnace	0.146	0.272	0.53	0.056	0.111	0.51
2	300 °C after furnace	0.012	0	–	0.001	0	–
3	900 °C before furnace	0.280	0.543	0.52	0.059	0.111	0.54
4	900 °C after furnace	0.446	0.440	1.01	0.005	0	–

The mass concentrations of CO_2 and H_2O were normalized to the aerosol mass concentration derived from SMPS volume and effective density ρ_{eff} .

[Title Page](#)
[Abstract](#)
[Introduction](#)
[Conclusions](#)
[References](#)
[Tables](#)
[Figures](#)
[Back](#)
[Close](#)
[Full Screen / Esc](#)
[Printer-friendly Version](#)
[Interactive Discussion](#)

**Hygroscopic and
cloud condensation
nuclei activation
properties**

D. F. Zhao et al.

[Title Page](#)[Abstract](#)[Introduction](#)[Conclusions](#)[References](#)[Tables](#)[Figures](#)[I◀](#)[▶I](#)[◀](#)[▶](#)[Back](#)[Close](#)[Full Screen / Esc](#)[Printer-friendly Version](#)[Interactive Discussion](#)**Table 4.** Growth factors at 90% RH, experiment under wet conditions.

Time after experiment start	GF(90%)
30 min	1.100
60 min	1.226
4.5 h	1.560
19.5 h	1.609

Hygroscopic and cloud condensation nuclei activation properties

D. F. Zhao et al.

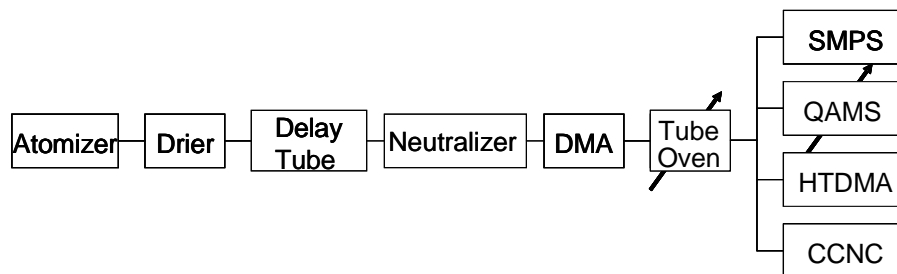


Fig. 1. Schematics of experimental set up. (Details see text.).

Title Page

Abstract

Introduction

Conclusions

References

Tables

Figures

◀

▶

◀

▶

Back

Close

Full Screen / Esc

Printer-friendly Version

Interactive Discussion

Hygroscopic and cloud condensation nuclei activation properties

D. F. Zhao et al.

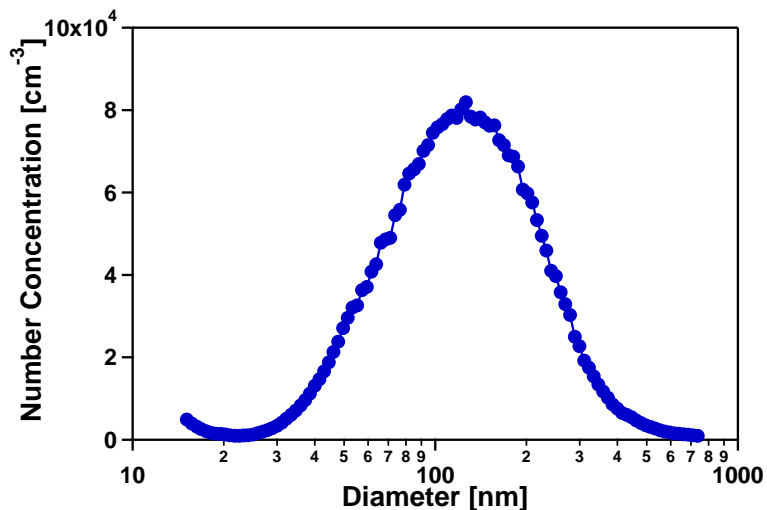


Fig. 2. Typical size distribution of aerosols generated by atomizing the $\text{Ca}(\text{HCO}_3)_2$ solutions with a TSI3076 constant output nebulizer. The aerosols were dried in a diffusion drier using Silica gel as desiccant.

Title Page

Abstract

Introduction

Conclusions

References

Tables

Figures

◀

▶

◀

▶

Back

Close

Full Screen / Esc

Printer-friendly Version

Interactive Discussion

**Hygroscopic and
cloud condensation
nuclei activation
properties**

D. F. Zhao et al.

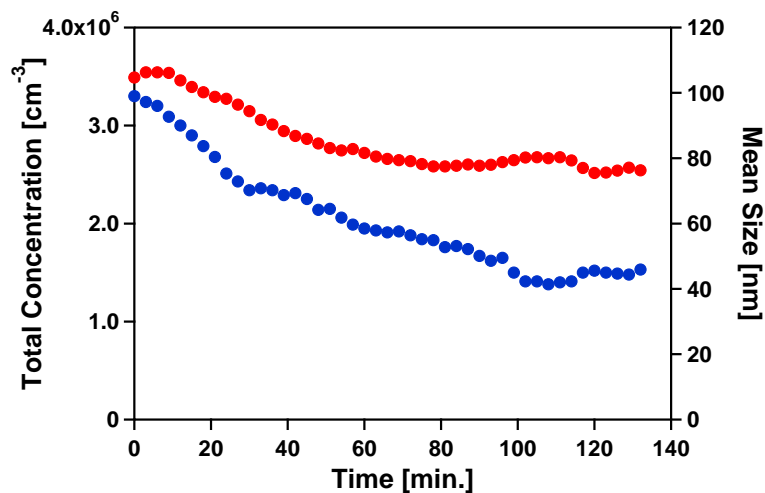


Fig. 3. Change with spraying time of the total number concentration (blue, left axis) and the mean size (red, right axis) of dry aerosols generated by atomizing $\text{Ca}(\text{HCO}_3)_2$ solution.

[Title Page](#)[Abstract](#)[Introduction](#)[Conclusions](#)[References](#)[Tables](#)[Figures](#)[◀](#)[▶](#)[◀](#)[▶](#)[Back](#)[Close](#)[Full Screen / Esc](#)[Printer-friendly Version](#)[Interactive Discussion](#)

Hygroscopic and cloud condensation nuclei activation properties

D. F. Zhao et al.

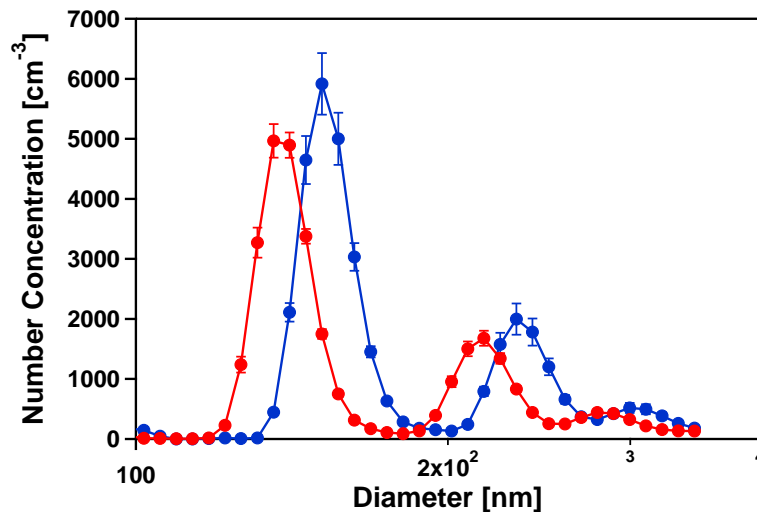


Fig. 4. Size distribution of neutralized, dry particles, electro-mobility selected at 150 nm, *before* (blue) and *after* (red) annealing at 300 °C in the tube furnace. The particles were generated by atomizing a $\text{Ca}(\text{HCO}_3)_2$ solution.

[Title Page](#)[Abstract](#)[Introduction](#)[Conclusions](#)[References](#)[Tables](#)[Figures](#)[⏪](#)[⏩](#)[◀](#)[▶](#)[Back](#)[Close](#)[Full Screen / Esc](#)[Printer-friendly Version](#)[Interactive Discussion](#)

Hygroscopic and cloud condensation nuclei activation properties

D. F. Zhao et al.

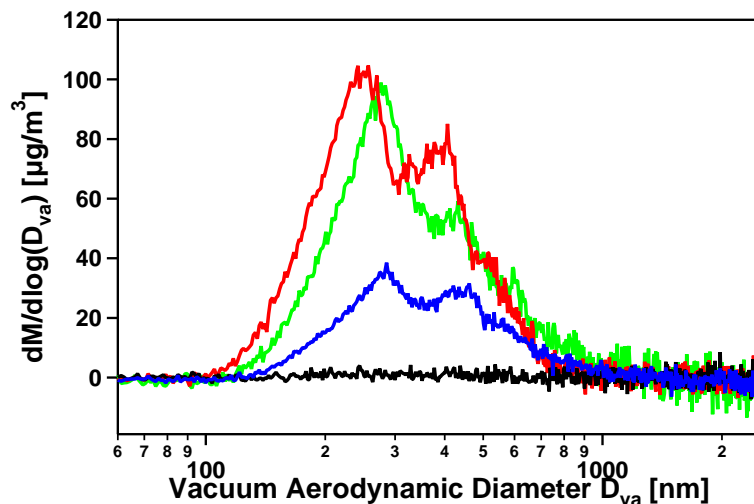


Fig. 5. Mass size distributions derived from the CO_2^+ signal in the pToF mode of the Q-AMS. Blue: aerosol *before annealing*, AMS vaporizer at 300°C (case 1), black: aerosol *after annealing* at 300°C , Q-AMS vaporizer at 300°C (case 2), green: aerosol *before annealing*, Q-AMS vaporizer 900°C (case 3), red: aerosol *after annealing* at 300°C , Q-AMS vaporizer 900°C (case 4).

[Title Page](#)[Abstract](#)[Introduction](#)[Conclusions](#)[References](#)[Tables](#)[Figures](#)[⏪](#)[⏩](#)[◀](#)[▶](#)[Back](#)[Close](#)[Full Screen / Esc](#)[Printer-friendly Version](#)[Interactive Discussion](#)

**Hygroscopic and
cloud condensation
nuclei activation
properties**

D. F. Zhao et al.

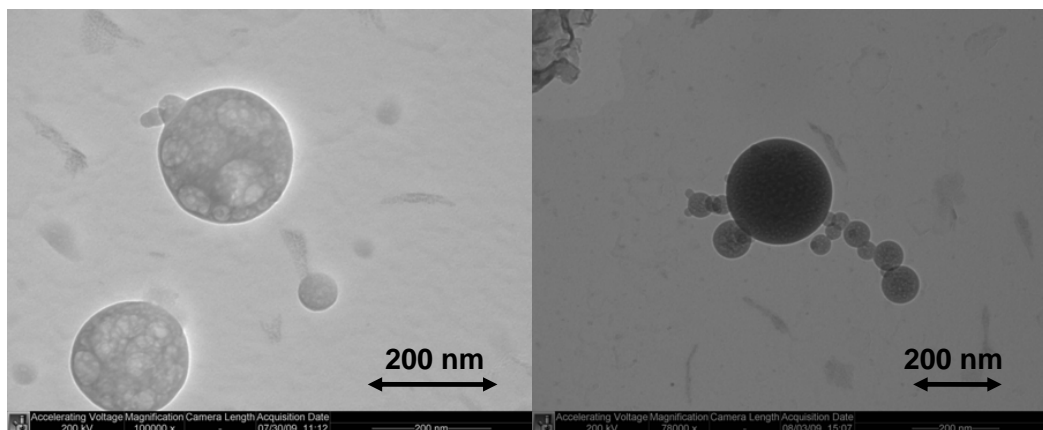
**(a)****(b)**

Fig. 6. TEM images of aerosol particles before **(a)** and after **(b)** annealing at 300 °C in the tube furnace. The aerosol particles were generated by atomizing the $\text{Ca}(\text{HCO}_3)_2$ solutions and dried before deposition on the TEM grids.

[Title Page](#)[Abstract](#)[Introduction](#)[Conclusions](#)[References](#)[Tables](#)[Figures](#)[◀](#)[▶](#)[◀](#)[▶](#)[Back](#)[Close](#)[Full Screen / Esc](#)[Printer-friendly Version](#)[Interactive Discussion](#)

Hygroscopic and cloud condensation nuclei activation properties

D. F. Zhao et al.

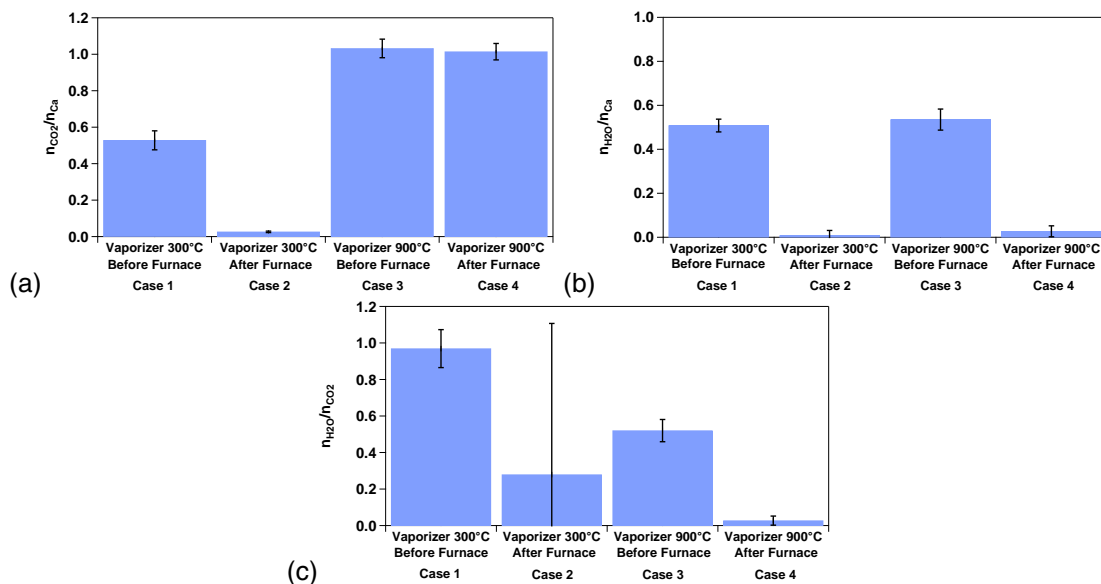


Fig. 7. Mole numbers of CO_2 (n_{CO_2}), **(a)**, H_2O ($n_{\text{H}_2\text{O}}$), **(b)** detected at different temperatures of the Q-AMS vaporizer before and after annealing in the tube furnace. The mole numbers of CO_2 and H_2O were derived by AMS and in (a) and (b) normalized to the Ca mole number (n_{Ca}) derived from SMPS measurements. The mole ratio $n_{\text{H}_2\text{O}}/n_{\text{CO}_2}$ **(c)** is based on AMS data only. Error bars are the standard deviations from repeated AMS measurements, respective the accordingly propagated errors in (c).

Title Page

Abstract

Introduction

Conclusions

References

Tables

Figures

◀

▶

◀

▶

Back

Close

Full Screen / Esc

Printer-friendly Version

Interactive Discussion

**Hygroscopic and
cloud condensation
nuclei activation
properties**

D. F. Zhao et al.

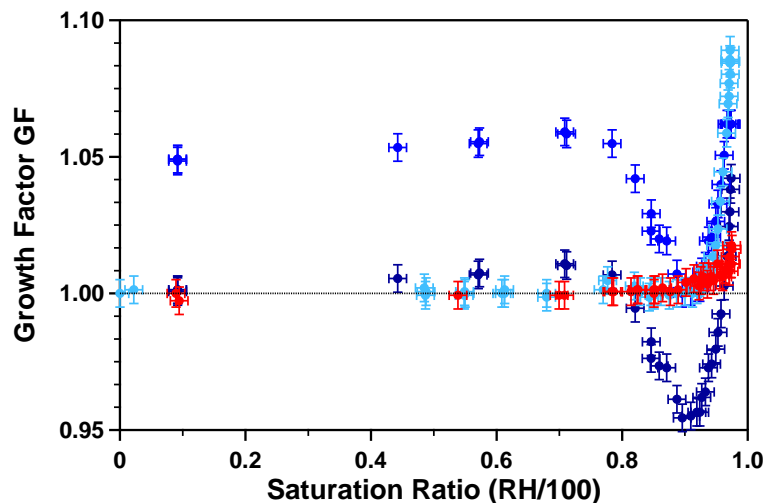


Fig. 8. Humidograms of calcium carbonate aerosols size selected at an electromobility diameter of 150 nm: red: CaCO_3 ; dark blue: $\text{Ca}(\text{HCO}_3)_2$; middle blue: $\text{Ca}(\text{HCO}_3)_2$ normalized to the minimum diameter at RH 89.5%; light blue: $\text{Ca}(\text{HCO}_3)_2$ processed with water before size selection (see text). Measurement errors: saturation ratio ± 0.014 , GF ± 0.005 .

[Title Page](#)[Abstract](#)[Introduction](#)[Conclusions](#)[References](#)[Tables](#)[Figures](#)[◀](#)[▶](#)[◀](#)[▶](#)[Back](#)[Close](#)[Full Screen / Esc](#)[Printer-friendly Version](#)[Interactive Discussion](#)

**Hygroscopic and
cloud condensation
nuclei activation
properties**

D. F. Zhao et al.

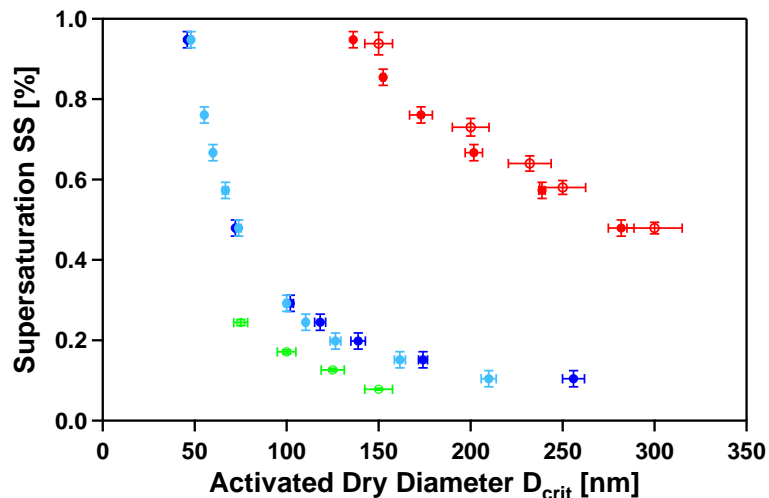


Fig. 9. Activated dry diameter for Ca(HCO₃)₂ (light blue) and CaCO₃ (red: solid symbols this study, open symbols Sullivan et al., 2009b), middle blue: Ca(HCO₃)₂ processed with water before size selection (see text); green: Ca(NO₃)₂ from Sullivan et al. (2009b).

[Title Page](#)[Abstract](#)[Introduction](#)[Conclusions](#)[References](#)[Tables](#)[Figures](#)[◀](#)[▶](#)[◀](#)[▶](#)[Back](#)[Close](#)[Full Screen / Esc](#)[Printer-friendly Version](#)[Interactive Discussion](#)

Hygroscopic and
cloud condensation
nuclei activation
properties

D. F. Zhao et al.

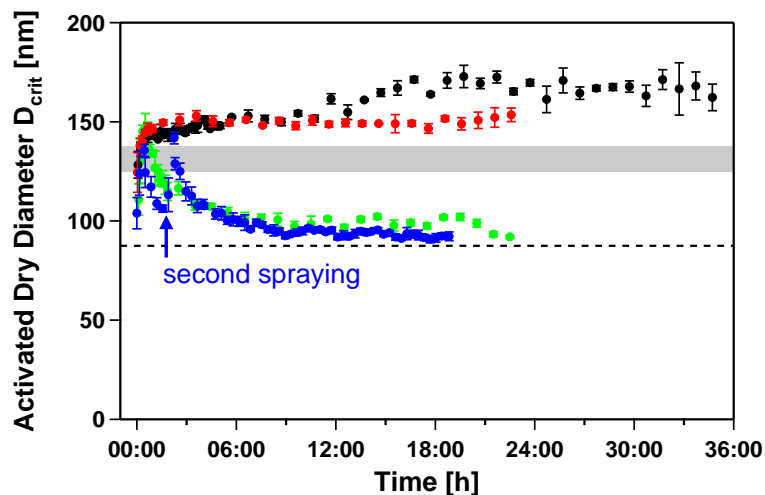


Fig. 10. Time series of activated dry diameters (D_{crit}) of calcium carbonate aerosols at 0.2% SS measured in the Large Aerosol Chamber filled with dry synthetic air (two experiments: red and black), with particle free outside air at $\sim 40\%$ RH (blue) and synthetic air at RH $\sim 40\%$ and 470 ppb NO_x (green), dashed line: $D_{\text{crit}}(\text{Ca}(\text{NO}_3)_2)$ by Sullivan et al. (2009b), grey area: $D_{\text{crit}}(\text{Ca}(\text{HCO}_3)_2)$ from this study. Error bars are the standard deviation of each measurement interval.

[Title Page](#)[Abstract](#)[Introduction](#)[Conclusions](#)[References](#)[Tables](#)[Figures](#)[◀](#)[▶](#)[◀](#)[▶](#)[Back](#)[Close](#)[Full Screen / Esc](#)[Printer-friendly Version](#)[Interactive Discussion](#)

Hygroscopic and cloud condensation nuclei activation properties

D. F. Zhao et al.

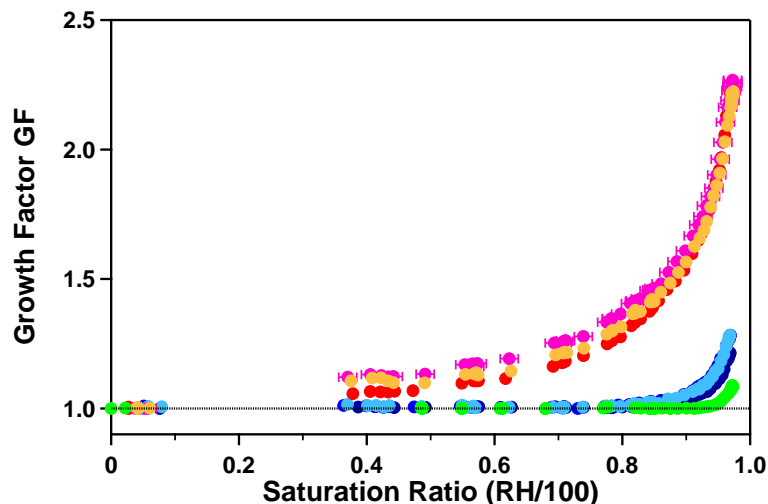


Fig. 11. Humidograms of calcium carbonate aerosols size selected at an electromobility diameter of 150 nm measured in the dry Large Aerosol Chamber (dark blue: after 1 h, middle blue: after 16 h, light blue: after 20 h). The same in the humidified Large Aerosols Chamber with 470 ppb NO_x added (red: after 3 h, pink: after 18 h, orange: after 20 h). For the measurements after 20 h the aerosol was additionally dried before entering the HTDMA. For comparison the humidogram of calcium carbonate aerosol pre-processed with water from the laboratory study. Measurement errors: saturation ratio 0.014, GF 0.005 (shown exemplary for one data set).

Title Page

Abstract

Introduction

Conclusions

References

Tables

Figures

◀

▶

◀

▶

Back

Close

Full Screen / Esc

Printer-friendly Version

Interactive Discussion

Hygroscopic and cloud condensation nuclei activation properties

D. F. Zhao et al.

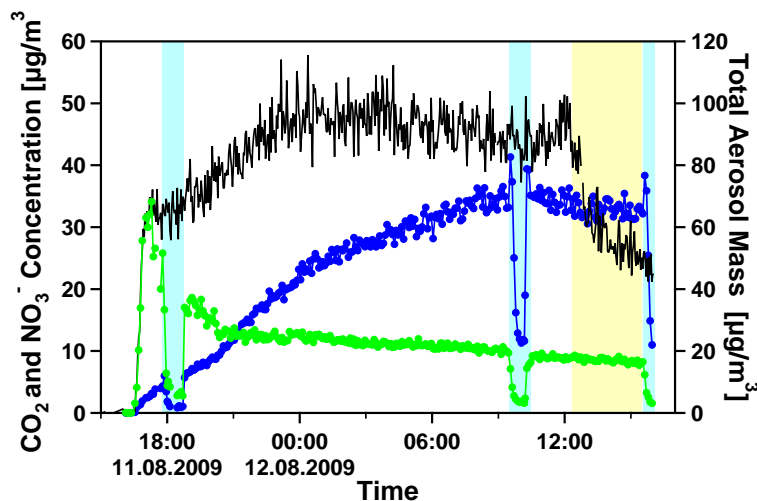


Fig. 12. Experiment in the humidified Large Aerosol Chamber with 470 ppb NO_x added. Time series of CO₂ (green, left axis), NO₃⁻ (blue, left axis) mass concentrations measured at 900 °C Q-AMS vaporizer temperature and total aerosol mass concentration (black, right axis) calculated from SMPS volume assuming a density of 1.8 g cm⁻³. Light blue areas: AMS vaporizer at 300 °C. Yellow area: the aerosol was dried with a silica gel diffusion drier before entering the Q-AMS.

Title Page

Abstract

Introduction

Conclusions

References

Tables

Figures

◀

▶

◀

▶

Back

Close

Full Screen / Esc

Printer-friendly Version

Interactive Discussion